

A study of the Al-rich region of the Al–Fe–Ir alloy system

B. Grushko

ERC-1, Forschungszentrum Jülich, 52425 Jülich, Germany

ARTICLE INFO

Keywords:

Aluminum alloys
Transition metal alloys and compounds
Phase diagrams

ABSTRACT

Phase equilibria in Al–Fe–Ir were studied at 850 and 1100 °C above 50 at% Al. The formation of the continuous ternary region of solid solutions was estimated along about 50 at% Al between the Al–Fe and Al–Ir β -phases. The binary $M\text{-Al}_{13}\text{Fe}_4$ and Al_5Fe_2 phases dissolve up to at least 10 and 5 at% Ir, the C_{Ir} -phase, Al_3Ir , χ_{Ir} -phase and Al_9Ir_2 up to ~ 4 , ~ 9 , ~ 2.5 and at least 2.5 at% Fe, respectively. These binaries extend to the ternary compositions at approximately constant Al. Three ternary phases designated m, L and N were revealed. The $m\text{-Al}_{13}(\text{Fe},\text{Ir})_4$ phase of the $\text{Al}_{13}\text{Os}_4$ -type structure ($C2/m$, $a = 1.7406$ nm, $b = 0.41923$ nm, $c = 0.76459$ nm, $\beta = 115.78^\circ$) is formed at $\sim \text{Al}_{75-76}\text{Fe}_{6-9}\text{Ir}_{18-15}$. A ternary hexagonal L-phase ($a = 1.09034$ nm, $c = 0.77614$ nm) is formed in a small compositional region around $\sim \text{Al}_{74}\text{Fe}_{14}\text{Ir}_{12}$. The structure of a complex ternary N-phase forming at $\sim \text{Al}_{77.5}\text{Fe}_{5.0-10.5}\text{Ir}_{17.5-12}$ was not specified.

1. Introduction

No ternary Al–Fe–Ir phase diagram has been yet published. On the other hand, the boundary binary Al–Fe and Al–Ir alloy systems have been extensively studied.

The Al-rich region of the Al–Fe alloy system, relevant to the present report, has been again specified in two contributions published synchronously without mutual mentions [1a,1b] and containing only some small differences in the configuration of the compositional regions of the phases.

The recent results concerning the Al–Ir phase diagram and its individual phases have been included in Ref. [2] and used in the studies of the ternary alloy systems of Al–Ir with Co and Rh [3].

In the present work, the phase equilibria in Al–Fe–Ir are studied in the compositional region above 50 at% Al at 850 and 1100 °C.

2. Experimental

Master alloys were produced by levitation induction melting in a water-cooled copper crucible under a pure Ar atmosphere. The purity of Al was 99.999%, of Fe 99.99%, of Ir 99.9%. Additional alloys of intermediate compositions were similarly produced from the mixtures of the residuals of the samples studied previously.

The as-cast specimens were annealed at 1100 °C under an Ar atmosphere (99.999% purity) or at 850 °C under vacuum (typically 9×10^{-7} mbar). The annealing times were up to 142 h at 1100 °C and up to 431 h at 850 °C. The as-cast and annealed samples were examined by powder

X-ray diffraction (XRD) and scanning electron microscopy (SEM). The compositions of the phases were measured by energy-dispersive X-ray analysis (EDX) in SEM on polished unetched surfaces (JEOL 840a scanning microscope equipped with EDAX Genesis 200 emission spectroscopy system). Powder XRD examinations were carried out using Cu $K\alpha_1$ radiation and an imaging plate (Huber G670). STOE software package was used for the indexing of the diffraction patterns and refinement of lattice parameters.

3. Results and discussion

3.1. Binary phases and their ternary extensions

The Al-rich region of the binary Al–Fe phase diagram in Fig. 1a is shown according to Ref. [1a]. All Al–Fe phases exhibit visible binary compositional regions. A CsCl-type structure forming in the Al–Fe alloy system around the equiatomic composition (β -phase) is an extension of the disordered solid solution of Al in bcc Fe whose melting temperature continuously decreases with the increasing Al concentration. The Al-rich part of the Al–Fe phase diagram also contains the equilibrium phases $M\text{-Al}_{13}\text{Fe}_4$, Al_5Fe_2 , Al_2Fe , and the high-temperature Al_8Fe_5 -phase. The crystallographic data of these phases are included in Table 1.

The Al-rich region of the Al–Ir phase diagram is shown in Fig. 1b according to Ref. [2], and around the equiatomic composition according to Ref. [4]. The congruent $\beta\text{-AlIr}$ phase melting at 2120 °C only extends towards lower Al at elevated temperatures. In the Al-rich region of Al–Ir, there are the phases $\theta\text{-Al}_9\text{Ir}_2$, $\varphi\text{-Al}_{45}\text{Ir}_{13}$, $\chi\text{-Al}_{28}\text{Ir}_9$ (χ_{Ir}), Al_3Ir and

E-mail address: b.grushko@fz-juelich.de.

<https://doi.org/10.1016/j.jalms.2023.100040>

Received 15 September 2023; Received in revised form 10 October 2023; Accepted 11 October 2023

Available online 12 October 2023

2949-9178/© 2023 The Author. Published by Elsevier B.V. This is an open access article under the CC BY license (<http://creativecommons.org/licenses/by/4.0/>).

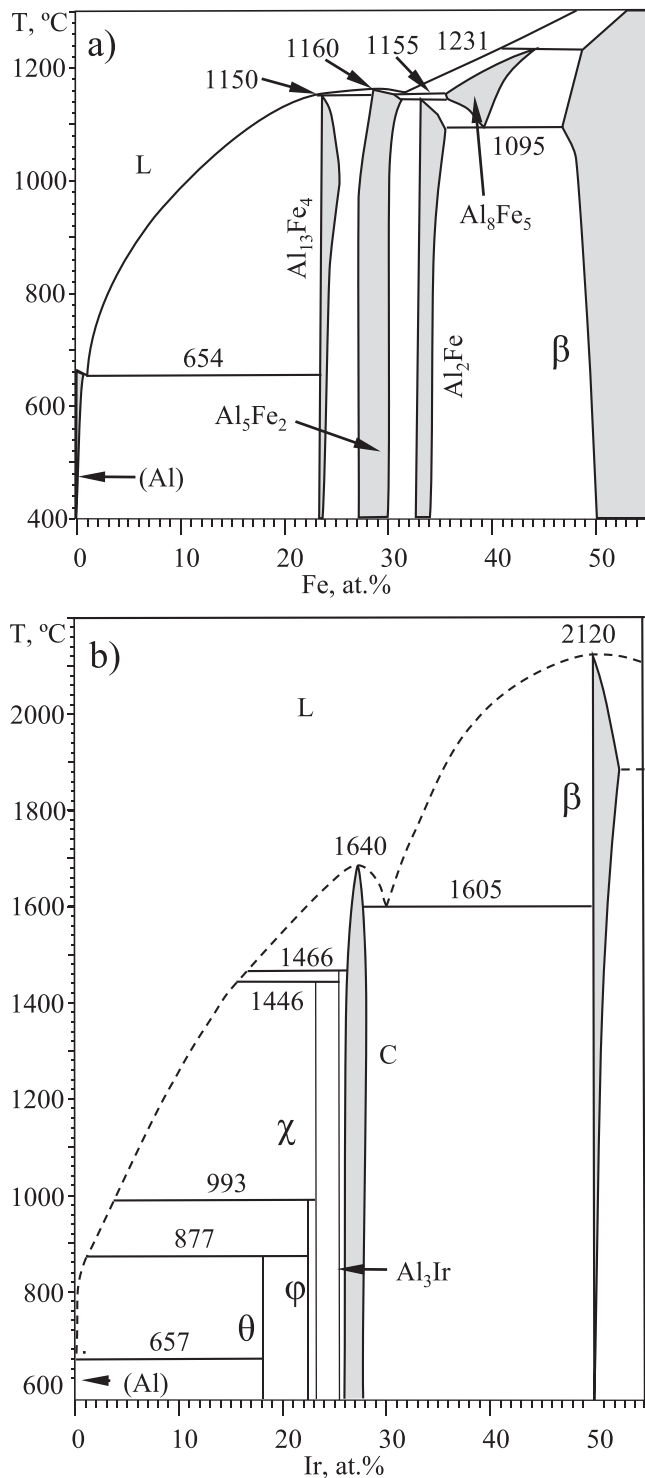


Fig. 1. Binary phase diagrams of: a) Al–Fe according to Ref. [1a], b) Al–Ir according to Refs. [2,4].

C-Al_{2.7}Ir (C_{Ir}) whose crystallographic data are included in Table 1.

Due to the existence of the isostructural Al–Fe and Al–Ir β-phases, the formation of the corresponding continuous ternary regions of solid solution is expected along about 50 at% Al. The β-phase containing Fe:Ir ≈ 1:1 was observed experimentally.

A ternary region extended from the M-Al₁₃Fe₄ phase was observed up to ~10 at% Ir, while the Al₅Fe₂ phase was found to dissolve up to ~5 at% Ir (see Fig. 2). Neither of alloys containing possible ternary extensions of Al₂Fe and Al₈Fe₅ were studied. The ternary extensions of

Table 1

Binary and ternary phases in Al–Fe–Ir mentioned in the text and diagrams. TW – this work.

Phase	Space group	Lattice parameters			Ref. Comment
		a, nm α, °	b, nm β, °	c, nm γ, °	
θ-Al ₉ Ir ₂	P2 ₁ /a	0.63779	0.64318 94.78	0.87337 -	[2]
φ-Al ₄₅ Ir ₁₃	Pnma	1.6771	1.2327	1.7437	[2]
χ-Al ₂₈ Ir ₉	P31c	1.2286	-	2.7375	[2]
Al ₃ Ir	P6 ₃ /mmc	0.4246	-	0.7756	[2]
		0.42185	-	0.77643	TW, (2)
		0.42216	-	0.77427	TW, Al _{73.5} Fe _{6.0} Ir _{20.5} (6)
		0.7674	-	-	TW, Al ₇₄ Fe ₉ Ir ₁₇ (8)
C-Al _{2.7} Ir	P23 or Pm3̄	0.76666	-	-	[2]
		(2)	-	-	TW, Al _{73.0} Fe _{4.5} Ir _{22.5}
β	Pm3̄m	0.28948	-	-	[1a], Al ₅₀ Fe ₅₀
		0.2985	-	-	[2], Al ₅₀ Ir ₅₀
M-Al ₁₃ Fe ₄	C2/m	1.5492	0.8078 107.69	1.2471 -	[1a]
		1.5509	0.8129	1.2522	TW, (3)
		-	(2)	(3)	Al _{75.5} Fe _{18.7} Ir _{5.8}
		-	107.77	-	(2)
		1.5497	0.8137	1.2495	TW, (3)
		-	107.64	-	Al _{76.0} Fe _{15.7} Ir _{8.3} (2)
Al ₅ Fe ₂	Cmcm	0.76559	0.64154	0.42184	[1a]
Al ₂ Fe	p1̄	0.48745	0.64545	0.87361	[1a]
		87.930	74.396	83.062	
Al ₈ Fe ₅	I43m	0.89757	-	-	[1a], at 1120 °C
m-Al ₁₃ (Fe, Ir) ₄	C2/m ^a	1.7406	0.41923	0.76459	TW, Al ₇₆ Fe ₈ Ir ₁₆ (2)
		-	115.78	-	(4)
		-	(7)	-	(6)
N	?	?	?	?	TW, Al _{77.5} Fe _{6.5} Ir ₁₆
L	P6 ₃ /m ^b	1.09034	-	0.77614	TW, (9)
		-	-	(5)	Al _{73.3} Fe _{13.5} Ir _{13.2}

^a S.G. is by analogy with the space group of the m-Al₁₃Os₄-phase [5].

^b S.G. is provisional.

the C_{Ir}-phase, Al₃Ir, χ_{Ir}-phase and Al₉Ir₂ were revealed along almost constant Al up to ~4, ~9, ~2.5 and at least 2.5 at% Fe, respectively.

3.2. Ternary phases and phase equilibria

Three ternary Al–Fe–Ir structures were revealed and designated in the following as N, m and L. The phase equilibria involving these ternaries and the above-mentioned binaries at 1100 °C and 850 °C are shown in Fig. 2a and b, respectively. The compositions of the phases forming in the studied alloys and the overall compositions of the alloys measured by SEM/EDX are marked in Fig. 2a, b by open squares and of by closed squares, respectively.

A single-phase sample was only obtained from the highest-Al N-phase (Al_{77.5}Fe_{6.5}Ir₁₆, see the powder XRD pattern in Fig. 3a), however the structures of the two other phases were easier encoded after the extraction of their powder XRD patterns from those in Fig. 3b and d, respectively.

The SEM/EDX examinations of a sample of Al_{76.7}Fe_{7.3}Ir₁₆ annealed at 1100 °C revealed a two-phase structure, where one of the phases exhibited the composition of the above-mentioned N-phase. By the subtraction of its powder XRD pattern (Fig. 3a) from that in Fig. 3b, the result indicated an Al₁₃Os₄-type monoclinic structure [5], which is also typical of the m-Al₁₃Co₄ phase [3,6]. The reliability of this identification of the m-Al₁₃(Fe, Ir)₄ phase was confirmed by a simulation of its powder

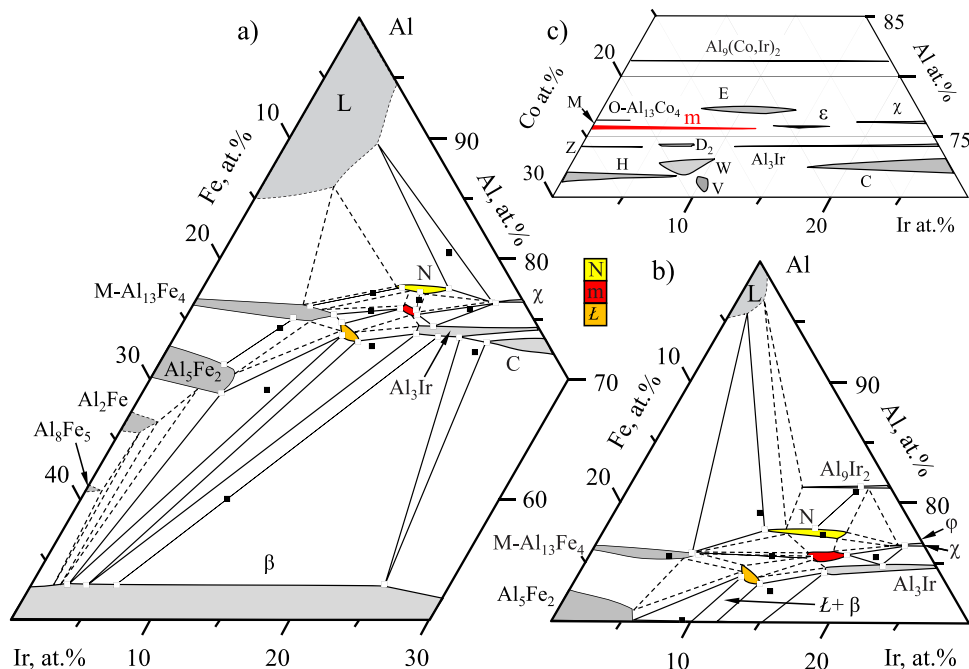


Fig. 2. Partial isothermal sections of Al–Fe–Ir at 1100 °C (a) and 850 °C (b); and the overall compositions of the Al-rich Al–Co–Ir phases at 850–1100 °C (c) drawn from the data of Ref. [3]. L is the liquid. The regions of the phases N, m and L are marked by yellow, red and orange, respectively. Provisional lines are shown broken. The measured compositions of the phases are marked by open squares and of the alloys by closed squares.

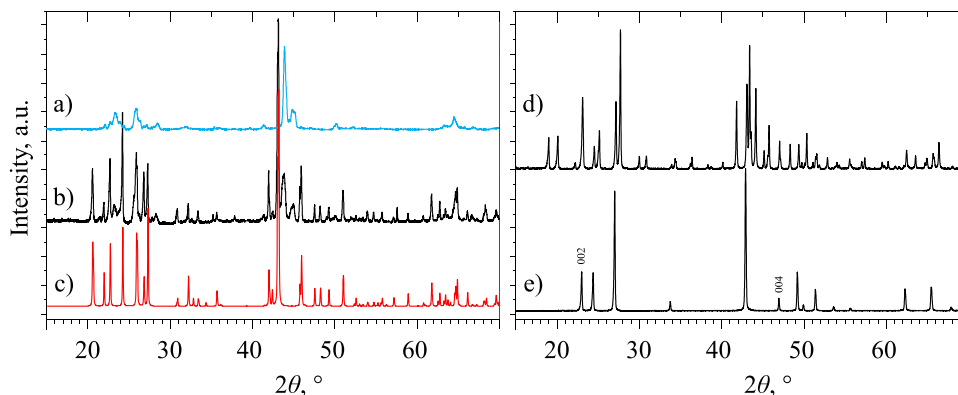


Fig. 3. Powder XRD patterns (Cu K α 1 radiation): a) of Al_{77.5}Fe_{6.5}Ir₁₆ annealed at 850 °C, b) of Al_{76.7}Fe_{7.3}Ir₁₆ annealed at 1100 °C; c) calculated from the structural model of the Al₁₃Os₄ m-phase of Ref. [5] using the refined lattice parameters of the Al–Fe–Ir m-phase; d) of Al_{72.7}Fe_{12.8}Pt_{14.5} annealed at 1100 °C, e) of Al₃Ir phase (the (00l) lines are marked, l = 2 n).

XRD pattern (see Fig. 3c) using the structural model of the m-Al₁₃Os₄ phase from Ref. [5]. The refined lattice parameters of the m-Al₁₃(Fe,Ir)₄ phase are included in Table 1.

The Al concentration of the m-Al₁₃(Fe,Ir)₄ phase, forming inside ~Al_{75–76}Fe_{6–9}Ir_{18–15}, is similar to that of the high-temperature m-Al₁₃Co₄ phase. The m-Al₁₃Co₄ phase was found to extend up to ~12 at% Ir (see Fig. 2c), but at the ternary compositions, equivalent to those of the m-Al₁₃(Fe,Ir)₄ phase, the orthorhombic ϵ_{16} -type structure (ϵ in Fig. 2c) was revealed in Al–Co–Ir [3]. The M-Al₁₃Fe₄ phase, which coexists with m-Al₁₃(Fe,Ir)₄ at its ternary extension, is isostructural to monoclinic M-Al₁₃Co₄, which coexists with the m-Al₁₃Co₄ phase in binary Al–Co [3,6]. However, no solubility of Ir was revealed in the M-Al₁₃Co₄ phase, while the orthorhombic O-Al₁₃Co₄ phase was found to dissolve some Ir (see Fig. 2c).

The ternary Al–Fe–Ir L-phase was not associated with any of the binary or ternary Al-based structures revealed to date. It is formed in a small compositional region around ~Al₇₄Fe₁₄Ir₁₂. The powder XRD pattern of an Al_{72.7}Fe_{12.8}Ir_{14.5} alloy containing the major L-phase is

shown in Fig. 3d. According to SEM/EDX this alloy also contained some Al₃(Ir,Fe), which could be easily recognized in the corresponding diffraction pattern, and the traces of β . Apart from the (00l) lines of Al₃(Ir,Fe) (see Fig. 3e) no other overlaps of the lines of this minor phase were revealed. After the subtraction of the diffraction lines of Al₃(Ir,Fe), the resulted pattern could be indexed for a hexagonal lattice (see Table 1 and Appendix).¹

The structure of the above-mentioned N-phase was not specified. This phase was revealed in a compositional range of ~Al_{77.5}Fe_{5.0–10.5}Ir_{17.5–12.0}, close to the equivalent compositions of the Al–Co–Ir E-phase [3] and Al–Ru–Rh E-phase [7] (see Fig. 4, upper panel). On the other hand, its powder XRD pattern exhibited more similarities to that of a ternary N-phase revealed recently in Al–Fe–Pt [8]

¹ Alternatively, the powder XRD pattern could be indexed using a primitive orthorhombic lattice of a two times smaller volume: $a = 0.94383(7)$ nm, $b = 0.77596(4)$ nm, $c = 0.54525(4)$ nm ($\Delta 2\theta = 0.008^\circ$, FOM(30) = 61.7).

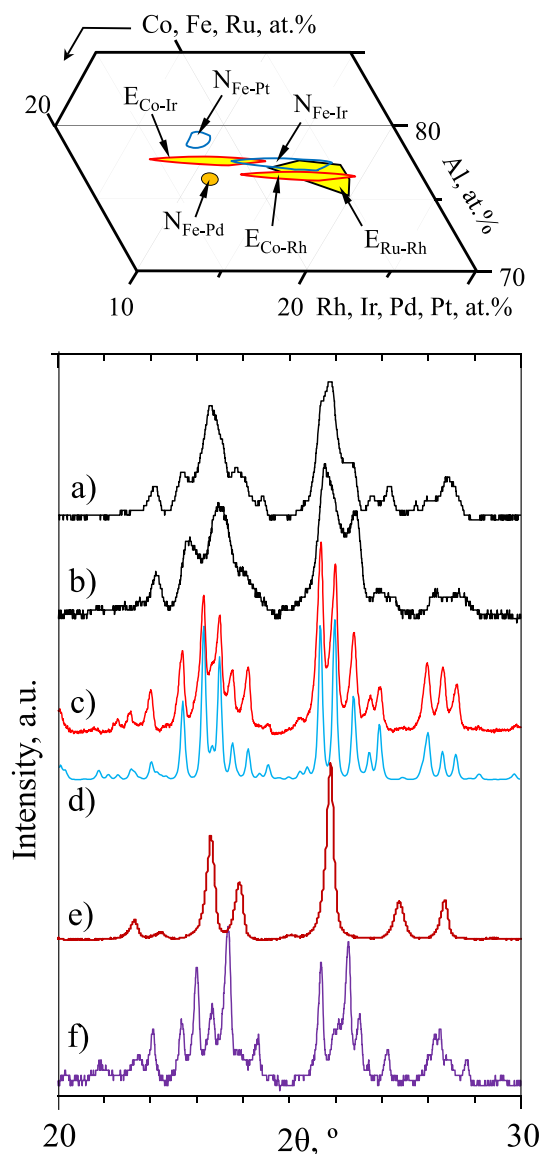


Fig. 4. Upper panel: overall compositions of the Al–Fe–Ir N-phase and the E-phases and N-phases mentioned in the text. Lower panel: selected 2θ regions of the powder XRD patterns (Cu K α 1 radiation) of: a) the $\text{Al}_{77.5}\text{Fe}_{6.5}\text{Ir}_{16}$ N-phase (same as in Fig. 3a), b) the $\text{Al}_{79}\text{Fe}_{12}\text{Pt}_9$ N-phase of Ref. [6], c) the $\text{Al}_{77}\text{Co}_{11}\text{Ir}_{12}$ E-phase of Ref. [3], d) calculated from the structural model of Ref. [7] for the refined lattice parameters of the E-phase in (c), e) the $\text{Al}_{78}\text{Ru}_{16}\text{Pt}_6$ D₄-phase [10], f) the $\text{Al}_{76.6}\text{Fe}_{13.4}\text{Pd}_{10.0}$ N-phase of Ref. [11].

around $\sim\text{Al}_{79}\text{Fe}_{12}\text{Pt}_9$ (see Fig. 4a, b vs. Fig. 4c). Subsequently it was also designated N. Attempts to index the powder XRD patterns of the both these N-phases using the structural model of the Al–Ru–Rh E-phase

published in Ref. [9] were not successful. In contrast, the powder XRD patterns of the Al–Co–Ir E-phase (Fig. 4c) and Al–Co–Rh E-phase were reliably indexed in Ref. [3] using the same structural model which is demonstrated by the comparison of the experimental and calculated diffraction patterns (see Fig. 4c,d). Similarly to that in the E-phases, the strong diffraction lines of the N-phases concentrate around the angular positions also typical of a decagonal phase with the periodicity of ~ 1.65 nm in the specific direction (D₄, see Fig. 4e [10]) pointing to the structural relation of these phases.

Another ternary orthorhombic phase, earlier revealed in Al–Fe–Pd [11], exhibited quite a similar powder XRD pattern (see Fig. 4f), where strong reflections are concentrated around the positions typical of the D₄-phase. This also-called N-phase is formed around a somewhat lower-Al composition (Fig. 4, upper panel). It was studied in Ref. [11] by powder XRD and electron diffraction. The corresponding lattice parameters $a \approx 2.31$, $b \approx 1.60$ nm are close to those of the E-phases ($a \approx 2.35$ nm, $b \approx 1.65$ nm), but $c \approx 4.70$ nm is more than twice larger than $c \approx 2.00$ nm of the E-phases. In contrast to the E-phases, no structural model of the Al–Fe–Pd N-phase was deduced yet. The Al–Fe–Pt N-phase of Ref. [8] was designated just *expecting* structural relation to that in Al–Fe–Pd, where Pt would mainly replace Pd.

4. Summary

- Phase equilibria in Al–Fe–Ir were studied at 850–1100 °C above 50 at% Al.
- The formation of the continuous ternary region of solid solutions was estimated along about 50 at% Al between the Al–Fe and Al–Ir β -phases.
- $\text{M-Al}_{13}\text{Fe}_4$ and Al_5Fe_2 dissolve up to at least 10 and 5 at% Ir, respectively.
- The C_{Ir} -phase, Al_3Ir , χ_{Ir} -phase and Al_9Ir_2 were found to extend along almost constant Al up to ~ 4 , ~ 9 , ~ 2.5 and at least 2.5 at% Fe, respectively.
- The study revealed the formation of three ternary phases designated m, L and N.
- The ternary m- $\text{Al}_{13}(\text{Fe},\text{Ir})_4$ phase of the $\text{Al}_{13}\text{Os}_4$ -type structure is formed at $\sim\text{Al}_{75-76}\text{Fe}_{6-9}\text{Ir}_{18-15}$.
- A ternary hexagonal L-phase is formed in a small compositional region around $\sim\text{Al}_{74}\text{Fe}_{14}\text{Ir}_{12}$.
- The structure of a complex ternary N-phase forming at $\sim\text{Al}_{77.5}\text{Fe}_{5.0-10.5}\text{Ir}_{17.5-12}$ was not specified.

Declaration of Competing Interest

The authors declare that they have no known competing financial interests or personal relationships that could have appeared to influence the work reported in this paper.

Acknowledgement

The author thanks C. Thomas for technical contributions.

Appendix

Diffraction data of the L-phase. S.G. = $P6_3/m$ (provisional). Refined lattice parameters: $a = 1.09034(9)$ nm, $c = 0.77614(5)$ nm. Aver. $\Delta 2\theta = 0.009^\circ$, Max. $\Delta 2\theta = 0.047^\circ$, FOM(30) = 81.8 from the total 54 lines. The sample contained minor Al_3Ir and traces of the β -phase, whose lines were excluded. The intensities marked by (*) are estimated due to the overlap with the reflections of Al_3Ir . The reflections with $I/I_0 < 5\%$ are not included.

No.	<i>h</i>	<i>k</i>	<i>l</i>	I/I_0	d, nm
1	2	0	0	22	0.47194
2	1	1	1	24	0.44608
3	0	0	2	12*	0.38803
4	2	1	0	28	0.35694
5	2	1	1	100	0.32431
6	2	0	2	9	0.29982
7	2	1	2	7	0.26260
8	3	1	0	5	0.26181
9	3	1	1	8	0.24812
10	3	1	2	48	0.21712
11	2	1	3	87	0.20949
12	4	1	0	31	0.20606
13	4	0	2	13	0.20168
14	3	0	3	10	0.19980
15	4	1	1	31	0.19916
16	0	0	4	7*	0.19405
17	3	2	2	18	0.18916
18	4	1	2	25	0.18203
19	4	2	1	8	0.17392
20	3	2	3	7	0.16609
21	4	2	2	5	0.16212
22	4	1	3	8	0.16118
23	3	1	4	5	0.15591
24	6	0	1	5	0.15422
25	4	2	3	9	0.14688
26	4	3	2	7	0.14409
	6	1	0		
27	4	1	4	19	0.14125
28	6	1	2	8	0.13497
	7	0	0		
	2	2	5		
29	4	4	1	5	0.13422
30	7	0	1	9	0.13289
31	7	0	2	6	0.12740
32	6	2	2	12	0.12403
	4	1	5		
33	3	0	6	8	0.11960
	7	0	3		

References

- [1] (a) Xiaolin Li, Anke Scherf, Martin Heilmaier, Frank Stein, J. Phase Equilib. Diffus 37 (2016) 162;
(b) K. Han, I. Ohnuma, R. Kainuma, J. Alloy. Compd. 668 (2016) 97.
- [2] D. Pavlyuchkov, B. Grushko, T.Ya Velikanova, Intermetallics 16 (2008) 801.
- [3] B. Grushko, J. Alloy. Compd. 772 (2019) 399.
- [4] C. Zhang, J. Zhu, Y. Yang, F. Zhang, Y.A. Ahang, Scr. Mater. 59 (2008) 403.
- [5] L.-E. Edshammar, Acta Chem. Scand. 18 (1964) 2294.
- [6] X.L. Ma, U. Köster, B. Grushko, Z. Krist. 213 (1998) 75.
- [7] B. Grushko, D. Kapush, T. Ya Velikanova, S. Samuha, L. Meshi, J. Alloy. Compd. 509 (2011) 8018.
- [8] B. Grushko, J. Alloy. Compd. 829 (2020), 154444.
- [9] S. Samuha, E. Mugnaioli, B. Grushko, U. Kolb, L. Meshi, Acta Crystallogr. B70 (2014) 999.
- [10] D. Kapush, S. Samuha, L. Meshi, T.Ya Velikanova, B. Grushko, J. Phase Equilib. Diffus. 36 (2015) 327.
- [11] S. Balanetsky, B. Grushko, T.Ya Velikanova, K. Urban, J. Alloy. Compd. 376 (2004) 158.